Computational Materials Science 179 (2020) 109642

Contents lists available at ScienceDirect

Computational Materials Science

journal homepage: www.elsevier.com/locate/commatsci

Nanoindentation of polycrystalline Pd hollow nanoparticles: Grain size role

Felipe J. Valencia[a,b,*], Benjamín Pinto[c], Miguel Kiwi[b,d], Carlos J. Ruestes[g], Eduardo M. Bringa[e,f], José Rogan[b,d]

[a] Centro de Investigación DAiTA Lab, Facultad de Estudios Interdisciplinarios, Universidad Mayor, Chile
[b] Centro para el Desarrollo de la Nanociencia y la Nanotecnología, CEDENNA, Avda. Ecuador 3493 Santiago, 9170124 Chile
[c] Escuela de Construcción, Universidad Mayor, Chile
[d] Departamento de Física, Facultad de Ciencias, Universidad de Chile, Casilla 653, Santiago 7800024, Chile
[e] CONICET and Facultad de Ingenieria, Universidad de Mendoza, Mendoza 5500, Argentina
[f] Centro de Nanotecnología Aplicada, Facultad de Ciencias, Universidad Mayor, Chile
[g] Instituto Interdisciplinario de Ciencias Básicas, Universidad Nacional de Cuyo, CONICET and Facultad de Ciencias Exactas y Naturales, Padre J. Contreras 1300, 5500 Mendoza, Argentina

ARTICLE INFO

Keywords:
Hollow nanoparticles
Nanoindentation
Polycrystalline materials
Plasticity

2010 MSC:
00-01
99-00

ABSTRACT

Polycrystalline hollow nanoparticles present a unique combination of strength and flexibility. However, the exact role displayed by their grain structure in mechanical properties has not been yet fully understood. Here, by means of molecular dynamics simulations, the role of grain boundary structure during the nanoindentation of metallic hollow nanoparticles with a polycrystalline shell was investigated. Our simulations were performed for a range of grain sizes and shell thicknesses, including the large strain regime. Our results show that hNP mechanical properties can be controlled by tuning the grain size of the polycrystalline shell, following an inverse Hall-Petch type dependence with the grain size. Deformation involves dislocation activity, twin hardening, grain boundary sliding, coalescence, and rotation. For single crystal shells at large strain there is hardenning following the closure of the internal cavity. For nanocrystalline shells at large strains a constant flow stress regime is observed even for deformations as high as 80%, thanks to grain boundary activity. Surprisingly, some particular grain size not only leads to an improvement in strength, but also a flow stress higher than the observed in their single-crystalline counterparts. Our work, suggest that grain boundary structure can be employed to improve and tailor desired mechanical properties in hollow nanostructures.

1. Introduction

The mechanical performance of nanocrystalline (NC) materials is often limited by their ductility [1]. To take advantage of their characteristic ultra-high strength in diverse scenarios it is necessary to look for novel architectures that help to overcome their current limitations [2–4]. In this pursuit, Shanet al. [5] converted a compact NC PdSe structure into a hollow nanosphere, resulting in lightweight, strong and highly deformable nanostructures. Similarly, Yang et al. [6,7] studied amorphous carbon hollow nanoparticles (hNP) under nanoindentation, achieving compressions of 30–50% before material failure; that is, deformations an order of magnitude larger than expected for amorphous carbon films [8]. Moreover, Si hollow nano- and micro-spheres, formed by single or colloidal arrays, have been suggested as lightweight nanoparticle protective films [9–11].

The ability to withstand large mechanical deformations seems to be a characteristic feature of hNPs, whose mechanical properties are known to differ significantly from bulk, and also with their non-hollow counterparts [12,13]. This behavior was addressed by atomistic simulations of Pd and Si hNPs, which show that the mechanical response can be properly controlled by geometrical parameters [14,15]. In fact, some convenient combinations of radius and shell thickness can improve simultaneously strength and flexibility. Interesting, this principle seems to be also exhibed in core shell NP, where Kilymiset al. [16] show that convenient shell thickness can delay the plastic deformation.

The cavity of single-crystal (sc) hollow nanostructures introduces additional degrees of freedom, allowing for surface buckling and stress redistribution on the hNP shell [14,15]. Considering that in NC materials the grain displacement or accommodation is often limited by the grain boundary density, the presence of a cavity can be thought as a route to enhance grain accommodation and flow. This principle was explored by Shanet al. [5]; however, in their experiments the exact

* Corresponding author at: Centro de Investigación DAiTA Lab, Facultad de Estudios Interdisciplinarios, Universidad Mayor, Chile.
E-mail address: felipe.valencia@umayor.cl (F.J. Valencia).

https://doi.org/10.1016/j.commatsci.2020.109642
Received 6 December 2019; Received in revised form 3 March 2020; Accepted 5 March 2020
Available online 18 March 2020
0927-0256/

mechanism at small and large deformations, and the role of the grain boundary structure [5] was not addressed.

Bulk NC display strengthening as the grain size decreases, in the Hall-Petch (HP) regime, often attributed to dislocation pile-up at grain boundaries. However, for grains smaller than 15–25 nm, usually there is an inverse HP regime, that is attributed to enhanced GB activity [1]. Understanding how these regimes apply to a hNP geometry is not trivial, partly because experimental dislocation identification at the nanoscale is difficult. Molecular Dynamics (MD) simulations can provide valuable information on the plastic deformation mechanism of hNP systems, complementing experiments. However, available simulations have dealt only with pristine, single crystal hNP shells, which are difficult to create with current synthesis techniques [14,15]. In fact, hNP synthesized by calcination, Kirkerdall effect, laser ablations, among others, are likely to be polycrystallines or porous [17]. All these features can bring about unexpected combinations of mechanical properties.

Here, using atomistic simulations, we investigate the nanoindentation response of metallic Pd hNP, with NC shells, as a possible route to improve both plasticity yielding and strength. The main focus of our work is to investigate if the grain boundary structure could be employed as an additional parameter to control the mechanical properties of hollow materials. Pd has been chosen due to the large amount of experimental evidence showing that Pd hNP are likely to be policrystaline [18–20], in with the same size-range studied here, together with Pd relevance as energy storage materials [21,22]. We expect that our study could be useful to improve the current Pd-based H storage technologies, which are often limited by the lack of ductility and strength of the available Pd membranes. [23].

2. Methods

The nanoindentation of metallic hNPs of NC shells is studied by means of molecular dynamics (MD) simulation, as implemented in the LAMMPS code [24]. The interaction between Pd atoms is simulated using the Embedded Atom Method potential [25], with the potential parameters by Sheng *et. al* [26]. This potential has shown to successfully reproduce experimental and DFT calculations of elastic constants [27], stacking fault (SF) and twin energies [28], the bulk modulus and the equation of state of Pd for pressures up to 100 GPa [29], among other properties. A good description of these parameters is requiered for the study of mechanical deformations of Pd.

Polycrystalline Pd samples, with the desired average grain size were created by a Voronoi tessellation algorithm [30]. NC samples were relaxed using the following procedure: first, atoms with energies larger than 50 eV, indicated some degree of overlap, were deleted from the simulation; next samples were relaxed using conjugate gradient coupled with a box relaxation to achieve zero pressure. To allow grain boundary re-accomodation the sample was annealed at a temperature of $T = 2T_m/3$, where T_m correspond to Pd melting temperature. The system temperature was controlled with a Nose-Hoover algorithm coupled to a zero pressure barostat during 20 ps. Finally, the sample was cooled during 0.2 ns down to 300 K. This procedure leads to a NC with a residual stress [31,32] as low as 10^{-5} GPa. Once the NC is relaxed, a hNP with the desired radius and thickness is obtained by carving this “bulk” Pd NC.

This cut will generate a hNP far from equilibrium, since some stress remnant is to be expected. Thus, the hNP is again relaxed during 0.5 ns at 300 K to allow grain boundary accommodation and surface reconstruction. This methodology has already been employed for the simulation of other metallic hNPs such as gold [33–35], silver [36], platinum [37] and palladium [22,38].

The indentation was performed using a repulsive flat indenter, with a harmonic potential of the form

$$U(z) = K(z - z_0)^3, \quad (1)$$

where z_0 is the indenter position, and $K = 10$ eV/Å^3 is the indenter stiffness.

Before indentation the relaxed hNP is situated on a fixed flat bottom surface with the same harmonic potential as the indenter. Next the hNP was relaxed in order to obtain a relaxed contact area with the bottom surface. No MD simulations of hNP on surfaces are available, and the only evidence of hNP contact is due to Jiang et al. [36], revealing that two hNPs can nucleate SFs due to the surface contact.

All hNPs studied here have an external radius of 10 nm, and a shell thickness ranging from 3 to 10 nm. The hNP were constructed from NCs with an average grain size $d = 5$, 7, and 10 nm. This allows to create hNPs with shells that have different grain boundary densities. The resulting hNPs have different mean grain size than the parent NC bulk structure.

Defect analysis [39] was carried out using the common neighbor analysis (CNA), implemented in OVITO [40]. Dislocations were identified with the DXA algorithm [41], and the defective atom count, such as in stacking faults or twin boundaries, was analyzed with the Crystal Analysis Tool (CAT) code. [41]. Strain calculations were also carried out with OVITO. Grain boundary rotations were identified with the local crystallographic orientation [42] (lco) algorithm implemented in the AACSD code. [43].

Stress-strain plots were obtained computing the atomistic contact area of the NC and the indenter. To obtain this area, we compute the number of indenter-NC atoms in contact using the method by Ziengehain *et. al* [44], defined by $|z - z_0| < 0.2$ Å, where z is the atom z-coordinate and z_0 the indenter position. The flow stress was defined as the stress (σ_{zz}) averaged within the 0.12 to 0.15 strain range.

3. Results

To characterize the hNP mechanical properties it is necessary to take into account all the possible relevant parameters that influence mechanical properties: grain size (d), shell thickness (t), and hNP radius (R). As a first step Fig. 1 addresses the role of the wall thickness for a $R = 10$ nm hNP, which was built from a nanocrystal of $d = 10$ nm average grain size. The macroscopic stress shows that hNPs of any thickness have similar mechanical behavior.

NC metal MD simulations[45–47] show a limited quasi-elastic regime, since GB activity leads to early plasticity. A stress maximum is reached, and thereafter a well defined flow stress is achieved slightly above 0.10 strain, after some softening. Only the results for $t = 3$–4 nm show some similarity with the bulk behavior. Larger t values display hardenning, suggesting that the geometry plays an important role in strengthtenning hNPs. This is consistent with recent simulations of related scenarios. Yuanet al. [48] simulated layer-grained models, with brick-like grains, and observed hardenning under tension caused by the formation of sessile dislocations due to reduction of dislocation motion.

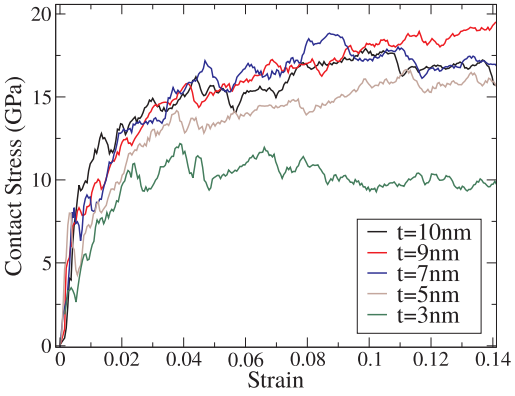

Fig. 1. Contact stress vs. strain for a 10 nm grain size hNP, for several different wall thicknesses.

hNP in our simulation also contain grains which are more flat than equiaxed due to the carving procedure, and many junctions are observed as deformation proceeds. Zahiriet al. [47] simulated bulk NC under compression, observing hardenning for NC with pre-existing twins, and stacking faults which lead to enhanced dislocation production. hNPs also contain some pre-existing dislocations, as will be shown below. Kianiet al. [49] used diffusive dynamics simulations to show the evolution under compression of Cu nanocubes with a Au precipitate inside. If the precipitate is impenetrable to dislocations significant hardenning is observed, in agreement with experiments. For hNPs dislocation motion is restricted by the hollow interior, with dislocations limited to cross grains and reach free surfaces.

The flow stress difference observed between $t = 3$ nm and t>5 nm suggests that hardening for larger thickness is due to the presence of a larger number dislocation junctions than for thinner shells. However, a dislocations inspection for $t = 10$ nm and $t = 3$ nm shows that junctions as $\frac{1}{3}\langle 100\rangle$ (Hirt), and $\frac{1}{6}\langle 110\rangle$ (Stair-Rod) make a contribution not larger than ~5% for both thicknesses. Major differences in dislocation plasticity were noticed for Shockley partial dislocations with ~74% for $t = 3$ nm, versus 58% for $t = 10$ nm, while full dislocation populations increase with thickness from 7% for $t = 3$ nm to 18% for $t = 10$ nm.

Fig. 2a shows the dependence of flow stress on shell thickness t, which appears to saturates for the larger t values studied here. This is consistant with an inverse Hall-Petch effect for grains/thickness below 15–25 nm. For bulk NCs this is due to GB activity, but here the cavity surface also influences strength (Fig. 2b). In fact, the relatively small shell thickness creates surface stresses that strongly influence both thermal and mechanical stability, even under small perturbations [50]. In addition, we also notice that contact pressures close to 17 GPa have been achieved in sc Pd hNPs [14], but at strains which are considerably smaller than the ones we observe here.

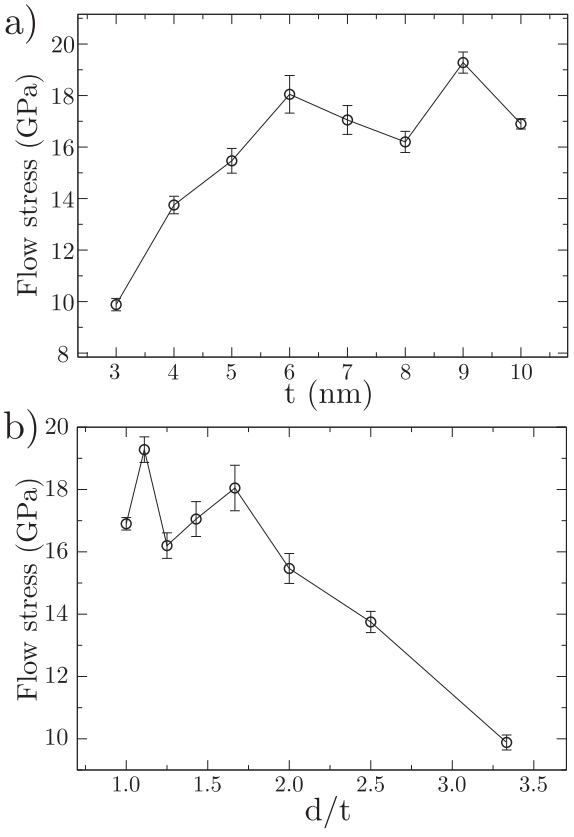

Fig. 2. (a) Flow stress as a function of wall thickness t, for 10 nm grain size. The flow stress was computed averaging the contact stress for strains in the 0.12 to 0.15 range. (b) Flow stress as a function of d/t.

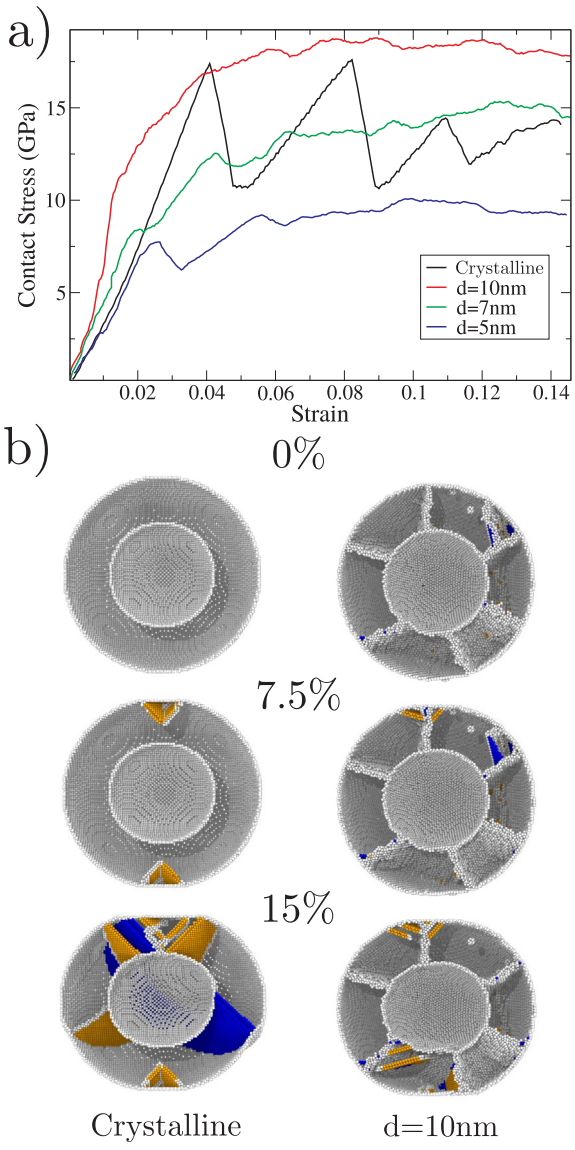

Fig. 3. (a) Contact stress for a $R = 10$ nm hNP of thickness $t = 5$ nm, for different grain sizes. The black line corresponds to a sc hNP. To obtain the statistics we averaged results of five different nanospheres. (b) Atomic distribution of a $d = 10$ nm hNP, for 0.0%, 7.5 and 15% compressions. Orange and blue atoms indicate that they belong to SF and twin boundaries, respectively. White atoms delimit the hNP surface and grain boundary structures, while fcc atoms are deleted from the figure.

To identify the role of the grain boundary structure the Fig. 3 shows the stress-strain relationship for hNPs with the same radii and thickness, but with different grain sizes. In all these cases, GB design leads to stresses which differ from sc systems [14,15] (black lines). The atomistic description provided by Fig. 3b clarifies the plastic deformation mechanisms governing each case. sc hNPs loaded along [001] are dominated by serrated behavior due to elastic hardenning followed by sudden activation of few preferential planes causing large stress drops. These dislocation bursts are dominated by partial dislocations and stacking faults along preferential {111} planes and become smaller as the NPs develop a network of SFs and twin boundaries.

Fig. 3a suggests that NC-hNPs tend to behave as a roughly isotropic material, which is reflected in a smooth stress-strain relation, with few abrupt drops in the plastic regime. NC-systems show evidence of SFs and twins in the vicinity of grain boundary junctions. Different grain orientaions make dislocation activity on different planes possible, but

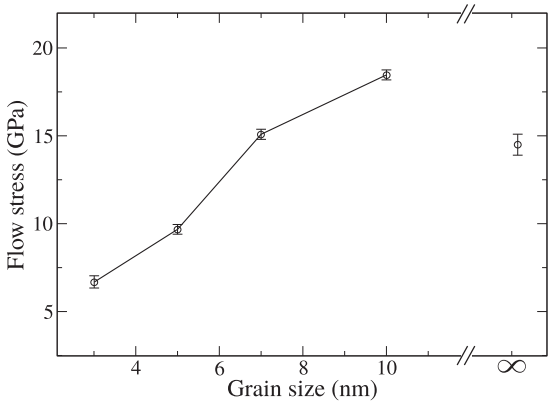

Fig. 4. Flow stress vs. grain size for a hNP with $R = 10$ nm and t = 5 nm. The stress flow was computed averaging over the range $\epsilon = 0.10$ to $\epsilon = 0.15$. The ∞ symbol in x axis corresponds to the sc hNP case.

now dislocations glide from one side of the grain to the other, instead of the longer glide across the whole shell thickness. We notice that the elastic limits are considerably smaller than for sc, due to GB activity, but the strengthening due to holds even for strains larger than $\epsilon = 0.15$, with grain size playing a dominant role in the stresses attained during the compaction. As expected from the inverse Hall-Petch regime we are simulating, the larger the grains the harder the NPs are. Shanet al. [5] observed experimentally that the strength of CdSe hNPs, with 6–8 nm grain size, differed significantly from the strength of bulk samples; however, the issue of the role of grain size was not explored further.

Here we find that larger stresses than for the single crystal case are achieved only for $d \leqslant 10$ nm, as seen in Fig. 4, for a shell thickness of 5 nm. The flow stress of sc hNP is ~3 GPa smaller than for the $d = 10$ nm case, which suggests the existence of an optimal grain size structure in the transition of inverse to conventional Hall-Petch strengthening, as for bulk NC.

Inverse Hall-Petch effect is usually associated to dominance of GB activity (sliding, rotation, reaccommodation), over dislocation slip. Dislocation density for different grain sizes (see Fig. 5) shows similar dislocaiton activity for 5, 7 and 10 nm grain sizes. The initial dislocation density is not zero, as in the single crystal case, because small dislocation embryos appear as a consequence of a NC relaxation process. The first significant dislocation slip events occur for $\epsilon = 0.025$, 0.06, and 0.075, for $d = 5$, 7 and 10 nm hNPs, respectively. Those strains are consistent with the yield onset of the respective stress-strain plots, and are attributed to the nucleation of Shockley partial dislocations mainly from grain boundary junctions. Stair-rod junctions or Hirth

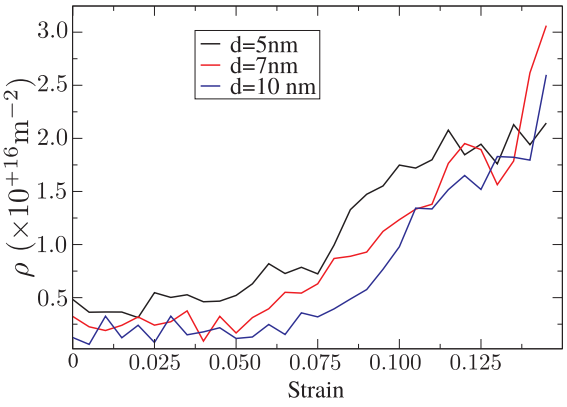

Fig. 5. Dislocation density vs. strain for a $R = 10$ nm and $t = 5$ nm hNP. Black, red, and blue correspond to 5 nm, 7 nm and 10 nm grain size, respectively. (For interpretation of the references to colour in this figure legend, the reader is referred to the web version of this article.)

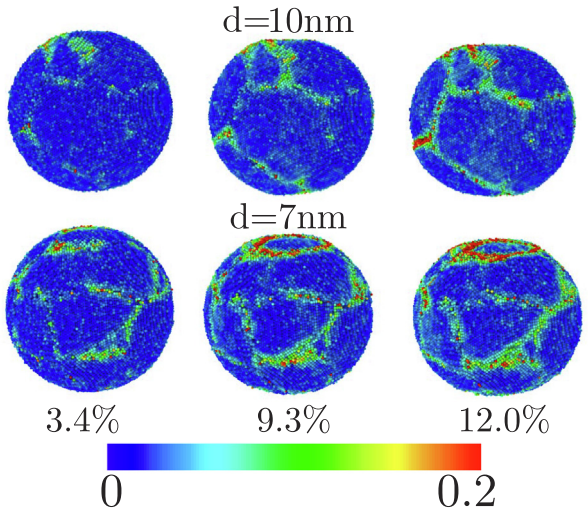

Fig. 6. External view of a hNP of $R = 10$ nm and $t = 5$ nm. Top panels correspond to a grain size of $d = 10$ nm, while bottom panels correspond to $d = 7$ nm. The color coding illustrates shear strain for different compressive strain. (For interpretation of the references to colour in this figure legend, the reader is referred to the web version of this article.)

partials, contributes less than 4% of the total dislocation lengths. Therefore, sessile dislocations are negligible, and no hardening is observed in the stress-strain plots of Fig. 3a.

The combination of hollow nanosphere design with grain boundary structure leads to more complex deformation modes than for conventional NC-systems. The hNP free volume allows for a richer grain boundary activity, which can be maintained for larger compressions than in a conventional NC bulk. Fig. 6 illustrates the shear strain of a hNP for three representative strains. For both grain sizes represented in the figure the most relevant shear activity does occur in the grain boundary region. For a 7 nm hNP the shear accumulation is larger than for $d = 10$ nm, which is to be expected as the grain boundary density is larger. It worth noticing that the largest shear zone is observed below the indenter contact zone; however, some shear accumulation can also be concentrated far from indenter region, in particular in triple junction zones. By plotting the shear-strain histograms of Fig. 1S one clearly observes an increase of sheared atoms in the tails of the distributions, which follow an inverse tendency with grain size (inset). Shear localization at grain boundaries will lead to enhanced grain boundary activity.

To provide a more detailed description of failure modes during the nanoindentaion of NC-hNPs, larger compressive strains were also achieved. Fig. 7 shows the contact pressure plot for two hNPs of thickness $t = 3$ nm and 5 nm, up to 80% compressions, respectively. Both exhibit a similar behavior, while at low strain (15%) there is hardening; this is followed by a constant stress regimen until strains 80%. Finally, the nanostrucure loses the hollow structure due to full compaction (vi and iii). The sc hNPs (green and blue) show smaller flow stress than their polycrystalline counterparts, since 10 nm grain size is relatively close to the Hall-Petch maximum. The stress-strain behavior displays some similarities with the one for nanoporous metals [51], where ligament size limits dislocation slip similarly to grain size. These metals also show nearly perfect plastic behavior, and porosity reduction leads to hardenning.

In order to describe the plastic behavior over different regimes Fig. 8 illustrates both SF and twin boundaries of representative regions. Stress reduction above 0.1 strain is consistent with the nucleation of several SF planes (i and iv). This is rather expected as SF planes are generally the trace the Shockley partial dislocation activity. Soon after that, twin populations display a noticeable increase during the constant stress regime, as illustrated in Fig. 8 (ii and v). Shell thickness is too

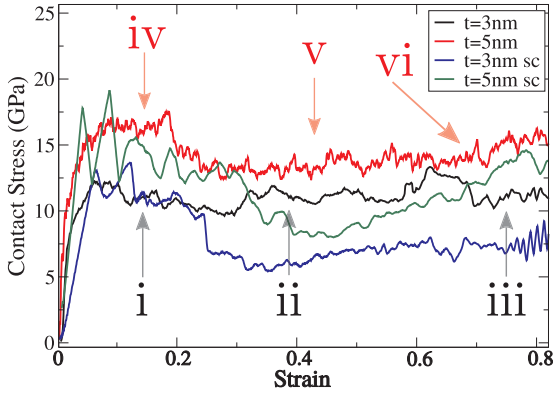

Fig. 7. a) Contact stress vs. strain for hNPs of external radius $R = 10$ nm, grain size $d = 10$ nm, and thicknesses $t = 3$ and $t = 5$ nm. Regions labeled i, ii, and iii correspond to representative plastic events for $t = 3$ nm, while iv, v, and vi correspond to $t = 5$ nm. Blue and green curve represent the sc hNP counterparts. (For interpretation of the references to colour in this figure legend, the reader is referred to the web version of this article.)

small to allow nucleation in multiple slip planes which would lead to dislocation junctions. The grain boundary structure and the relatively large surface area provide potential dislocation sinks. However, this is not always the case, since twin boundaries can act as a barrier for the free displacement of Shockley partial dislocations (iii and vi). Interestingly, when inner surfaces made contact a large number of SF are generated due to a surface reconstruction process, which is reflected in Fig.2S as a peak in the SF plot below 0.5 strain. Partial contact at the inner surface is followed up by increasing contact and elimination of porosity, creating a finite-size nanocrystal which can harden due to dislocation junctions in the compact material, as it happens for nanofoams [51].

We notice that for hNPs the small shell thickness dislocation activity is not the only source contributing to plasticity; in fact, the presence of the outer and inner surfaces can enhance GB activity. We observe that the activity is mainly assisted by displacement of adjacent grains, or by grain boundary rotation (Fig. 3S). Interestingly, grain rotation at room temperature has been already disscused as the dominant plastic deformation mode [52] in thin films. Here, a hNP can be thought of as a particular case of a thin film material which favors grain boundary mechanisms for plastic deformation, even at room temperature.

4. Conclusions

By means of molecular dynamics simulations we investigate the compression of nanocrystalline Pd hollow nanoparticles during nanoindentation with planar indenters. The mechanical properties were studied for different grain sizes and wall thicknesses, as well as in the small and large strain regimes. Our results suggest that hollow nanoparticle mechanical properties can be tailored by controlling their wall thickness and grain size, to obtain enhanced strength and ductility.

Plastic deformation is qualitatively similar to the one for bulk nanocrystals. There is an inverse Hall-Petch effect with grain size, d, but also with shell thickness for $t < d$. Grain boundary activity starts at low strain, and continues contributing at large deformations, thanks to the additional degrees of freedom provided by the free surfaces which can roughen and buckle. Additionally, partials dislocations nucleate from grain boundary junctions, cross the grains, and can contribute to twinning. This behavior differs with single-crystal hollow nanoparticles where dislocations can travel over the whole shell, without being stopped or absorbed by grain boundary [14,15].

Interesting, nanocrystalline hollow nanoparticles do not show the maximum stress peak observed in nanocrystalline bulks, and they show hardening even after the shell collapses. In addition, grain size and shell thickness can be chosen to give a flow stress significantly larger than for single-crystal hollow nanoparticles. Interesting, the constant flow stress regimen can be held even for strains larger than 70%, before the inner cavity finally collapses.

The hollow nanoparticles considered here are not larger than 20 nm and somewhat smaller than some experimental nanoshells. However, those experimental hollw nanoparticles will likely have shell thickness of the order of the grain size [53,17,5]. Since grain boundary density can be introduced as an additional parameter to control their mechanical properties, we expect that grain boundary engineering could be employed to improve and taylor desired mechanical properties not only in hollow nanoparticles, but also in other hollow nanostructures such as nanoframes [54], nanocages [55], foam-like structures [56], metallic nanotubes [57], and nanoparticle aerogels [58].

Data Availability

The raw/processed data required to reproduce these findings cannot be shared at this time due to technical or time limitations.

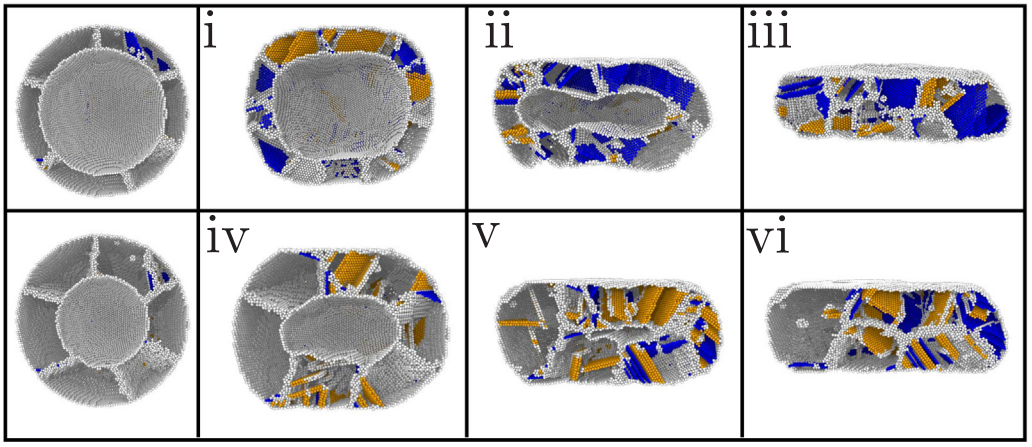

Fig. 8. Top panels illustrate the indentation process for a hNP of $t = 3$ nm, $R = 10$ nm, and grain size $d = 10$ nm. The bottom panels represent the compression of a $t = 5$ nm hNP. Frames i, ii, iii show representative snapshots of the hNP, while iv, v and vi display relevant plastic events. White atoms denote the grain boundary region, and the inner/outer surfaces. Orange and blue atoms depict atoms belonging to SF and twin boundaries, respectively. The fcc atoms were deleted. (For interpretation of the references to colour in this figure legend, the reader is referred to the web version of this article.)

CRediT authorship contribution statement

Felipe J. Valencia: Writing - original draft, Formal analysis. **Benjamín Pinto:** Formal analysis. **Miguel Kiwi:** Writing - review & editing, Methodology, Conceptualization. **Carlos J. Ruestes:** Writing - review & editing, Conceptualization. **Eduardo M. Bringa:** Writing - review & editing. **José Rogan:** Writing - review & editing.

Declaration of Competing Interest

The authors declare that they have no known competing financial interests or personal relationships that could have appeared to influence the work reported in this paper.

Acknowledgments

This work was supported by the Fondo Nacional de Investigaciones Científicas y Tecnológicas (FONDECYT, Chile) under grants #1160639 (MK) and 1190662 (JR and FV), FONDECYT de Iniciación #11190484 (FV), AFOSR Grant FA9550-16-1-0122, and Financiamiento Basal para Centros Científicos y Tecnológicos de Excelencia AFB180001 (FV, MK and JR). EMB thanks support from grants PICT-2014-0696 (ANPCyT) and M003 (SeCTyP-UN Cuyo). Powered@NLHPC: this research was partially supported by the supercomputing infrastructure of the NLHPC (ECM-02).

Appendix A. Supplementary data

Supplementary data associated with this article can be found, in the online version, athttps://doi.org/10.1016/j.commatsci.2020.109642.

References

[1] M.A. Meyers, A. Mishra, D.J. Benson, Mechanical properties of nanocrystalline materials, Prog. Mater Sci. 51 (4) (2006) 427–556.
[2] P.V. Liddicoat, X.-Z. Liao, Y. Zhao, Y. Zhu, M.Y. Murashkin, E.J. Lavernia, R.Z. Valiev, S.P. Ringer, Nanostructural hierarchy increases the strength of aluminium alloys, Nature Commun. 1 (2010) 63.
[3] D. Jang, L.R. Meza, F. Greer, J.R. Greer, Fabrication and deformation of three-dimensional hollow ceramic nanostructures, Nat. Mater. 12 (10) (2013) 893.
[4] R.O. Ritchie, The conflicts between strength and toughness, Nat. Mater. 10 (11) (2011) 817.
[5] Z. Shan, G. Adesso, A. Cabot, M. Sherburne, S.S. Asif, O. Warren, D. Chrzan, A. Minor, A. Alivisatos, Ultrahigh stress and strain in hierarchically structured hollow nanoparticles, Nature Mater. 7 (12) (2008) 947–952.
[6] W. Yang, S. Mao, J. Yang, T. Shang, H. Song, J. Mabon, W. Swiech, J.R. Vance, Z. Yue, S.J. Dillon, et al., Large-deformation and high-strength amorphous porous carbon nanospheres, Sci. Rep. 6 (2016) 24187.
[7] W. Yang, J. Yang, Y. Dong, S. Mao, Z. Gao, Z. Yue, S.J. Dillon, H. Xu, B. Xu, Probing buckling and post-buckling deformation of hollow amorphous carbon nanospheres: In-situ experiment and theoretical analysis, Carbon 137 (2018) 411–418.
[8] S. Cho, I. Chasiotis, T.A. Friedmann, J.P. Sullivan, Young's modulus, poisson's ratio and failure properties of tetrahedral amorphous diamond-like carbon for mems devices, J. Micromech. Microeng. 15 (4) (2005) 728.
[9] J. Yin, M. Retsch, E.L. Thomas, M.C. Boyce, Collective mechanical behavior of multilayer colloidal arrays of hollow nanoparticles, Langmuir 28 (13) (2012) 5580–5588.
[10] J. Yin, M. Retsch, J.-H. Lee, E.L. Thomas, M.C. Boyce, Mechanics of nanoindentation on a monolayer of colloidal hollow nanoparticles, Langmuir 27 (17) (2011) 10492–10500.
[11] L. Zhang, M. D'Acunzi, M. Kappl, G.K. Auernhammer, D. Vollmer, C.M. van Kats, A. van Blaaderen, Hollow silica spheres: synthesis and mechanical properties, Langmuir 25 (5) (2009) 2711–2717.
[12] A. Sharma, J. Hickman, N. Gazit, E. Rabkin, Y. Mishin, Nickel nanoparticles set a new record of strength, Nature Commun. 9 (1) (2018) 4102.
[13] J. Bian, L. Yang, X. Niu, G. Wang, Orientation-dependent deformation mechanisms of bcc niobium nanoparticles, arXiv preprint arXiv:1709.05526.
[14] F.J. Valencia, R.I. González, H. Vega, C. Ruestes, J. Rogan, J.A. Valdivia, E.M. Bringa, M. Kiwi, Mechanical properties obtained by indentation of hollow pd nanoparticles, J. Phys. Chem. C 122 (43) (2018) 25035–25042.
[15] L. Yang, J. Bian, H. Zhang, X. Niu, G. Wang, Size-dependent deformation mechanisms in hollow silicon nanoparticles, AIP Adv. 5 (7) (2015) 077162.
[16] D. Kilymis, C. Gérard, L. Pizzagalli, Ductile deformation of core-shell si-sic nanoparticles controlled by shell thickness, Acta Mater. 164 (2019) 560–567.
[17] M. Ibanez, J. Fan, W. Li, D. Cadavid, R. Nafria, A. Carrete, A. Cabot, Means and limits of control of the shell parameters in hollow nanoparticles obtained by the kirkendall effect, Chem. Mater. 23 (12) (2011) 3095–3104.
[18] G. Nie, X. Lu, J. Lei, L. Yang, X. Bian, Y. Tong, C. Wang, Sacrificial template-assisted fabrication of palladium hollow nanocubes and their application in electrochemical detection toward hydrogen peroxide, Electrochim. Acta 99 (2013) 145–151.
[19] H. Tianou, W. Wang, X. Yang, Z. Cao, Q. Kuang, Z. Wang, Z. Shan, M. Jin, Y. Yin, Inflating hollow nanocrystals through a repeated kirkendall cavitation process, Nature Commun. 8 (1) (2017) 1261.
[20] G. Fu, M. Gong, Y. Tang, L. Xu, D. Sun, J.-M. Lee, Hollow and porous palladium nanocrystals: synthesis and electrocatalytic application, J. Mater. Chem. A 3 (44) (2015) 21995–21999.
[21] H. Idrissi, B. Wang, M.S. Colla, J.P. Raskin, D. Schryvers, T. Pardoen, Ultrahigh strain hardening in thin palladium films with nanoscale twins, Adv. Mater. 23 (18) (2011) 2119–2122.
[22] F.J. Valencia, R.I. González, D. Tramontina, J. Rogan, J.A. Valdivia, M. Kiwi, E.M. Bringa, Hydrogen storage in palladium hollow nanoparticles, J. Phys. Chem. C.
[23] T.B. Flanagan, W. Oates, The palladium-hydrogen system, Annu. Rev. Mater. Sci. 21 (1) (1991) 269–304.
[24] S. Plimpton, Fast parallel algorithms for short-range molecular dynamics, J. Comp. Phys. 117 (1) (1995) 1–19, https://doi.org/10.1006/jcph.1995.1039.
[25] M.S. Daw, M.I. Baskes, Embedded-atom method: Derivation and application to impurities, surfaces, and other defects in metals, Phys. Rev. B 29 (12) (1984) 6443.
[26] H. Sheng, M. Kramer, A. Cadien, T. Fujita, M. Chen, Highly optimized embedded-atom-method potentials for fourteen fcc metals, Phys. Rev. B 83 (13) (2011) 134118.
[27] G. Simmons, H. Wang, Single Crystal Elastic Constants and Calculated Aggregate Properties, MIT Press, Cambridge, Mass, 1971.
[28] W. Tyson, W. Miller, Surface free energies of solid metals: estimation from liquid surface tension measurements, Surf. Sci. 62 (1) (1977) 267–276.
[29] H. Mao, P. Bell, J.T. Shaner, D. Steinberg, Specific volume measurements of cu, mo, pd, and ag and calibration of the ruby r1 fluorescence pressure gauge from 0.06 to 1 mbar, J. Appl. Phys 49 (6) (1978) 3276–3283.
[30] E. Bringa, J. Monk, A. Caro, A. Misra, L. Zepeda-Ruiz, M. Duchaineau, F. Abraham, M. Nastasi, S. Picraux, Y. Wang, et al., Are nanoporous materials radiation resistant? Nano Lett. 12 (7) (2011) 3351–3355.
[31] F. Valencia, J.D. Mella, R.I. Gonzalez, M. Kiwi, E.M. Bringa, Confinement effects in irradiation of nanocrystalline diamond, Carbon 93 (2015) 458–464.
[32] C.J. Ruestes, A. Stukowski, Y. Tang, D. Tramontina, P. Erhart, B. Remington, H. Urbassek, M.A. Meyers, E.M. Bringa, Atomistic simulation of tantalum nanoindentation: effects of indenter diameter, penetration velocity, and interatomic potentials on defect mechanisms and evolution, Mater. Sci. Eng.: A 613 (2014) 390–403.
[33] L. Jiang, X. Yin, J. Zhao, H. Liu, Y. Liu, F. Wang, J. Zhu, F. Boey, H. Zhang, Theoretical investigation on the thermal stability of hollow gold nanoparticles, J. Phys. Chem. C 113 (47) (2009) 20193–20197.
[34] L. Jiang, W. Sun, Y. Gao, J. Zhao, Geometric thermal phase diagrams for studying the thermal dynamic stability of hollow gold nanoballs at different temperatures, Phys. Chem. Chem. Phys. 16 (14) (2014) 6623–6629.
[35] S.S. Dalgic, Size dependent properties of hollow gold nanoparticles: a theoretical investigation, Acta Phys. Polonica A 129 (4) (2016) 531–534.
[36] S. Jiang, Y. Zhang, Y. Gan, Z. Chen, H. Peng, Molecular dynamics study of neck growth in laser sintering of hollow silver nanoparticles with different heating rates, J. Phys. D: Appl. Phys. 46 (33) (2013) 335302.
[37] A. Shan, Z. Chen, B. Li, C. Chen, R. Wang, Monodispersed, ultrathin nipt hollow nanospheres with tunable diameter and composition via a green chemical synthesis, J. Mater. Chem. A 3 (3) (2015) 1031–1036.
[38] F.J. Valencia, R.I. González, J.A. Valdivia, M. Kiwi, E.M. Bringa, J. Rogan, Inducing porosity on hollow nanoparticles by hypervelocity impacts, J. Phys. Chem. C 121 (33) (2017) 17856–17861.
[39] M.L. Falk, J.S. Langer, Dynamics of viscoplastic deformation in amorphous solids, Phys. Rev. E 57 (6) (1998) 7192.
[40] A. Stukowski, Visualization and analysis of atomistic simulation data with ovito-the open visualization tool, Modell. Simul. Mater. Sci. Eng. 18 (1) (2010) 015012http://stacks.iop.org/0965-0393/18/i=1/a=015012.
[41] A. Stukowski, Structure identification methods for atomistic simulations of crystalline materials, Modell. Simul. Mater. Sci. Eng. 20 (4) (2012) 045021.
[42] J.F. Panzarino, T.J. Rupert, Tracking microstructure of crystalline materials: a post-processing algorithm for atomistic simulations, Jom 66 (3) (2014) 417–428.
[43] Z. Liu, R. Zhang, Aacsd: an atomistic analyzer for crystal structure and defects, Comput. Phys. Commun. 222 (2018) 229–239.
[44] G. Ziegenhain, H.M. Urbassek, A. Hartmaier, Influence of crystal anisotropy on elastic deformation and onset of plasticity in nanoindentation: a simulational study, J. Appl. Phys. 107 (6) (2010) 061807.
[45] D. Bachurin, P. Gumbsch, Accommodation processes during deformation of nanocrystalline palladium, Acta Mater. 58 (16) (2010) 5491–5501.
[46] D. Bachurin, Influence of internal stresses on deformation behavior of nanocrystalline palladium, Mater. Sci. Eng.: A 734 (2018) 255–259.
[47] A.H. Zahiri, P. Chakraborty, Y. Wang, L. Cao, Strong strain hardening in ultrafast melt-quenched nanocrystalline cu: the role of fivefold twins, J. Appl. Phys. 126 (7) (2019) 075103.
[48] L. Yuan, P. Jing, R. Shivpuri, C. Xu, Z. Xu, D. Shan, B. Guo, Atomistic simulation of the stacking fault energy and grain shape on strain hardening behaviours of fcc nanocrystalline metals, Phil. Mag. 99 (22) (2019) 2818–2840.
[49] M.T. Kiani, Y. Wang, N. Bertin, W. Cai, X.W. Gu, Strengthening mechanism of a single precipitate in a metallic nanocube, Nano letters 19 (1) (2018) 255–260.
[50] P.N. Reyes, F.J. Valencia, H. Vega, C. Ruestes, J. Rogan, J. Valdivia, M. Kiwi, The

stability of hollow nanoparticles and the simulation temperature ramp, Inorganic Chem. Front. 5 (5) (2018) 1139–1144.
[51] C.J. Ruestes, D. Farkas, A. Caro, E.M. Bringa, Hardening under compression in au foams, Acta Mater. 108 (2016) 1–7.
[52] L. Wang, J. Teng, P. Liu, A. Hirata, E. Ma, Z. Zhang, M. Chen, X. Han, Grain rotation mediated by grain boundary dislocations in nanocrystalline platinum, Nature Commun. 5 (2014) 4402.
[53] K. Zhang, T. Holloway, A. Wingfield, J. Pradhan, W. Cao, A.K. Pradhan, Hollow gold nanospheres: growth morphology, composition and absorption characteristics, Micro Nanosystems 3 (1) (2011) 76–82.
[54] G.S. Métraux, Y.C. Cao, R. Jin, C.A. Mirkin, Triangular nanoframes made of gold and silver, Nano Lett. 3 (4) (2003) 519–522.
[55] S.E. Skrabalak, J. Chen, Y. Sun, X. Lu, L. Au, C.M. Cobley, Y. Xia, Gold nanocages: synthesis, properties, and applications, Acc. Chem. Res. 41 (12) (2008) 1587–1595.
[56] I. Vukovic, S. Punzhin, Z. Vukovic, P. Onck, J.T.M. De Hosson, G. ten Brinke, K. Loos, Supramolecular route to well-ordered metal nanofoams, ACS Nano 5 (8) (2011) 6339–6348.
[57] J. Rojas-Nunez, F. Valencia, R.I. Gonzalez, E.M. Bringa, S. Allende, J.L. Palma, A. Pereira, J. Escrig, S.E. Baltazar, Mechanical performance of lightweight polycrystalline ni nanotubes, Comput. Mater. Sci. 168 (2019) 81–86.
[58] N.C. Bigall, A.-K. Herrmann, M. Vogel, M. Rose, P. Simon, W. Carrillo-Cabrera, D. Dorfs, S. Kaskel, N. Gaponik, A. Eychmüller, Hydrogels and aerogels from noble metal nanoparticles, Angew. Chem. Int. Ed. 48 (51) (2009) 9731–9734.